Check for updates

Probing hydrogel microstructure and porosity with fluorinated liquid NMR nanocapsules

Ida Bochert,[ab] Camila M. Vacas Betancourt,[b] Dimitris Missirlis, [ID][ab] Nicolás Moreno-Gómez [ID] *[ab] and Peer Fischer*[abcd]

Characterizing the microstructure and porosity of hydrogels in their fully hydrated state remains a major challenge. We present a robust platform based on pulsed field gradient (PFG) NMR combined with 200 nm, liquid-filled nanocapsules to non-invasively measure mesh sizes of hydrogels. By explicitly accounting for particle polydispersity, the method enables accurate interpretation of PFG NMR data. Fluorinated reporter molecules in the liquid core enable the background-free detection *via* fluorine-19 (^{19}F) NMR in proton-rich polymer matrices. The microstructure of methacrylated hyaluronic acid (HAMA) hydrogels of varying concentrations is determined *via* PFG NMR diffusion measurements of the nanocapsules. A clear, HAMA concentration-dependent decrease in mesh size is observed and estimates of the mesh size are obtained using the liquid-core nanocapsules. This approach offers a non-destructive means to probe porous soft materials, offering a valuable tool for the characterization of hydrogels and complex soft tissues.

1 Introduction

The diffusion of micro- and nanoparticles through soft, disordered environments is of major importance for drug delivery applications in biological tissues and to understand the function of biomaterials like hydrogels.[1–5] Diffusion not only governs transport but also serves as a probe for underlying particle-environment interactions, revealing critical insights into the microstructure of porous and inhomogenous media.

Biogenic gels such as mucus or the extracellular matrix, as well as synthetic hydrogels, are examples of materials that give rise to complex diffusion effects. These materials form dense and dynamic polymer networks that restrict motion through steric hindrance, hydrodynamic resistance, and transient non-covalent interactions.[6–11] Tracking how particles navigate these networks can provide information on the gel microstructure and thereby the mesh size.

To determine nanoparticle diffusion, optical methods, such as fluorescence correlation spectroscopy, dynamic light scattering, or single particle tracking are widely used.[12] However, their utility falls short in opaque and heterogeneous media, as they

require fluorescent labeling and often only measure a limited number of particles.[12–14]

Pulsed-field gradient (PFG) NMR, in contrast, offers a non-invasive alternative. It has the key advantage of operating independently of optical transparency or fluorescent labeling, thus having the potential to probe diffusion in opaque, heterogeneous, and even crowded biological environments. PFG NMR measures large ensembles and yields diffusion coefficients directly, without relying on additional models. It is widely used for molecular systems and arguably can be considered the gold standard for studying molecular diffusion in complex media.[10,11,15–24] However, its use at the colloidal scale has been a longstanding challenge. The main reason is that for solid particles anisotropic dipolar couplings dominate, causing broadening of peaks, suppressing spin mobility and shortening relaxation times, making the NMR signal overall hard to detect.[12,25–27]

One way to overcome NMR signal loss from dipolar coupling in solid particles and to obtain a "sharp" signal that can be tracked for diffusion measurement is to use mobile molecules physically associated with the particles. Over long timescales, these molecules move with the particle and act as diffusion reporters. Two main strategies follow this principle: attaching flexible polymers to the particle surface,[28–31] or using particles with liquid cores.[30–42] Coatings like PEG polymers allow the detection in this case, but hinder further chemical modification of the particle surface, which is critical to understand interactions with the external environment. In this regard, the second approach of using liquid cores is more general,

[a] Max Planck Institute for Medical Research, Jahnstraße 29, 69120 Heidelberg, Germany. E-mail: Nicolas.Moreno@mr.mpg.de, Peer.Fischer@mr.mpg.de

[b] Institute for Molecular Systems Engineering and Advanced Materials, Heidelberg University, Im Neuenheimer Feld 225, 69120 Heidelberg, Germany

[c] Center for Nanomedicine, Institute for Basic Science (IBS), Seoul 03722, Republic of Korea

[d] Department of Nano Biomedical Engineering (NanoBME), Advanced Science Institute, Yonsei University, Seoul 03722, Republic of Korea

but its success depends on the stability of the core–shell colloids. Liposomes, for example, often leak, such that the signal of the tracer molecules is not reliably connected to the particle movement. This reduces their use in more viscous or complex environments, where longer diffusion and hence observation times are needed.[30–34]

Liquid-filled, polymer-shelled particles (nanocapsules) offer a more stable alternative, preventing leakage and enabling reliable tracking *via* their mobile liquid cores.[36] This makes them strong candidates as NMR diffusion probes. However, they are typically produced at micron scale, where diffusion is too slow for nanoscale transport studies using non-invasive PFG NMR. Their dimensions are also too big for most natural and synthetic hydrogels which are characterized by sub-micron mesh sizes. As a result, their use has been limited to flow-assisted setups.[35–41] One study has tested liquid-core particles in polymer foams at high volume fractions (15–45%), which affected the rheological properties.[39]

Here, we prepared hexadecane-filled poly(methyl methacrylate) (PMMA) nanocapsules with a diameter of about 200 nm and employed them as mobile probes to characterize hydrogels using PFG NMR. The measurement principle, illustrated in Fig. 1a, relies on a two-step confinement strategy. First, fast-diffusing reporter molecules (*e.g.*, hexadecane or a perfluorosilane) are confined within the nanocapsule solid polymer shell. While their motion at very short times is fast, at longer timescales their apparent mean squared displacement (MSD) is governed by the much slower movement of the nanocapsule that contains them (Fig. 1b). This allows us to use the signal as a precise proxy to measure the diffusion of the entire particle (Fig. 1c). When the nanocapsule is confined within the polymer network of a hydrogel, then the diffusion of the particle is further restricted by the surrounding mesh. At sufficiently long observation times, its MSD will plateau at a maximum value dictated by the dimensions of the cavity it is trapped in.

The value of this MSD "plateau" thus provides a direct measure for calculating the hydrogel mesh size.

In order to apply the nanocapsules to hydrogels and biological media, we chose a fluorine-19 (^{19}F) reporter molecule. This provides a superior, background-free signal in hydrogen-rich media, like hydrogels. Importantly, the nanocapsules we designed are of a similar size to extracellular vesicles or many drug carriers,[43–46] making them useful as NMR model particles. To demonstrate this, we examine the diffusion of our nanocapsules in agarose and methacrylated hyaluronic acid (HAMA) hydrogels.

Lastly, we show how these measurements allow us to estimate the mesh size of hydrogels in their native state. Existing methods determine this property using electron microscopy, which suffers from dehydration artifacts and limited penetration depth.[47,48] Other approaches including scattering,[48] rheology,[48,49] or swelling-experiments,[9,50–53] are indirect and model-dependent. In contrast, our approach uses nanoparticle diffusion as a direct, non-invasive probe of the hydrogel microstructure, providing access to mesh size under native conditions and in bulk media.

2 Material and methods

2.1 Materials

Poly(methyl methacrylate) (PMMA, Sigma-Aldrich, MW 350 000), hexadecane (HD, Sigma-Aldrich, 99%), dichloromethane (DCM, Carl-Roth, 99%), 1*H*,1*H*,2*H*,2*H*-perfluorooctyltriethoxysilane (Sigma, 98%), and sodium dodecyl sulfate (SDS, SERVA Electrophoresis GmbH, Research Grade), were used as received without further purification. Glycerol was purchased from Merck. Low-melting temperature agarose powder was purchased from Lonza Rockland, Inc. (NuSieve® GTG® Agarose). Sodium hyaluronate (100 kDa) was purchased from Lifecore Medical. Lithium phenyl-2,4,6-trimethyl-benzoylphosphinate (LAP) was purchased from TCI. Methacrylic
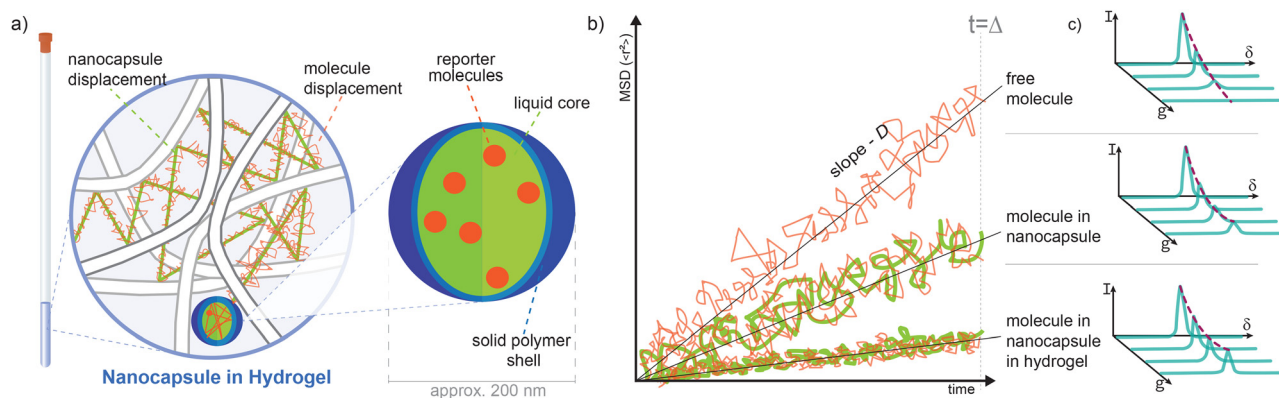

Fig. 1 Schematic explanation of the measurement principle: (a) nanocapsules act as diffusion probes, which can be measured by PFG NMR due to their liquid core. While the liquid molecules diffuse inside the particle core, they also follow the translational motion of the particle which diffuses in a complex environment. From the signal of the molecules in the liquid core, the diffusion of the particle can be determined. (b) By investigating the MSD of the molecules, one can distinguish between free and trapped molecules, with the latter representing the diffusion coefficient of the nanocapsules. If the capsule is restricted in its motion due to the microstructure of the medium (hydrogel), the diffusion is further slowed down. (c) By measuring the NMR peak intensity as a function of increasing gradient strength, the diffusion coefficient of the nanocapsules can be determined from the signal of the liquid core.

anhydride was purchased from Sigma. Phosphate buffered saline (PBS) was purchased from Gibco. Type 1 ultrapure water was obtained from a Lab Water Purification System.

2.2 Particle fabrication

The following procedure is adapted from the literature[54–56] and modified in order to fabricate smaller particles. PMMA-hexadecane nanocapsules with liquid cores and solid shells were fabricated using an internal phase separation method optimized for PFG NMR measurements. First, 0.1 g of sodium dodecyl sulfate (SDS) was dissolved in 50 g of water to prepare a 0.2% aqueous surfactant solution. Separately, 0.166 g of PMMA was dissolved in 4.582 g of dichloromethane (DCM), followed by the addition of 0.25 g of hexadecane and 100 µl of 1H,1H,2H,2H-perfluorooctyltriethoxysilane (POTS). The mixture was gently stirred to form a uniform organic phase. Using an ultrasound homogenizer (cycle 0.5, amplitude 100%), the SDS solution was stirred while the organic phase was slowly added over 60 seconds to form a stable oil-in-water emulsion. To reduce foaming, 0.25 g of acetone was added, followed by 40 seconds of additional ultrasonication to reduce particle size to the nanometer scale. To further stabilize the dispersion, 7.5 g of aqueous surfactant solution was added, resulting in a milky emulsion. The mixture was transferred to a crystallization dish and left overnight in a fume hood to allow for DCM evaporation. As PMMA has low solubility in hexadecane, its phase separation during solvent removal led to the formation of a solid PMMA shell around the liquid hexadecane core.

2.3 Sample preparation

For all measurements, except for the measurements in agarose gel, the particles were diluted to 5×10^{11} particles per ml, which corresponds to a volume fraction of around 0.15% (depending on the exact particle size). For the agarose measurements, the concentration was roughly 2×10^{12} particles per ml. Using this concentration, the effect of particle–particle interactions can be estimated to be negligible.

For nanoparticle tracking analysis (NTA) measurements, the particle stock solution was diluted by a factor 10^4, for dynamic light scattering (DLS) by factor 1000.

The samples of PMMA-hexadecane particles in glycerol were diluted in aqueous solutions containing 0, 20, 40, 60, 80% v/v of glycerol.

For the samples with particles in agarose gel, a higher concentrated agarose stock solution was prepared by dissolving the agarose powder in water and heating the solution to its boiling point. The required amount of agarose was added to the diluted particles. To prevent the final hot liquid from gelling in the NMR tube, both sample container and NMR tube were heated before transferring the sample to the NMR tubes using a pipette.

The HAMA polymers were obtained by functionalization of hyaluronic acid using the following protocol in analogy to the literature.[57] 100 kDa sodium hyaluronate was dissolved in MilliQ water to obtain a concentration of 1% w/v. The pH was adjusted to 9 and monitored during continuous and vigorous stirring. A $5\times$ molar excess of methacrylic anhydride was slowly added. Due to phase separation, the solution turned opaque. To keep the pH between 7 and 9, 1 N NaOH was regularly added. After 2.5 h, the mixture was centrifuged and hyaluronic acid methacrylate was precipitated using a $5\times$ volume excess of cold acetone. Afterwards, cold acetone was used for washing the precipitate (two times). The precipitate was dissolved in MilliQ water and lyophilized. The resulting white powder was stored at $-20\ ^{\circ}$C. For the gel preparation, a stock solution of 4% w/v in PBS buffer was used. The degree of functionalization was 14% as investigated using ^{1}H NMR. The NMR spectrum further revealed a small amount of methacrylic anhydride in the product. The effect for the final mass ratio of the polymer in the gel samples can be estimated to be negligible.

The HAMA gel samples were prepared by mixing HAMA polymer, particles, and LAP (photoinitiator). Gel concentrations of 0.8%, 1.0%, and 1.2% were prepared. The photoinitiator was always added to reach a final concentration of 2.5 mg ml^{-1}. The samples were illuminated with UV light at 405 nm for one minute.

2.4 Size and concentration measurements

The size of PMMA-hexadecane particles suspended in water was measured by DLS and NTA. The DLS measurements were performed on a Malvern Zetasizer Nano Z using a scattering angle of 173° and a temperature of 25 °C. Ten measurements were recorded to calculate the number-weighted hydrodynamic diameter. The NTA measurements were performed on a Nanosight NS300 from Malvern Panalytical. The installed sCMOS camera records videos with a frame rate of 25 frames per s. A laser wavelength of 488 nm was used. The temperature was set to 20 °C. Two measurements of 3 min were recorded using a flow speed of 2.4 µl s^{-1}. The camera level was set to 11, the detection threshold was 10, and a blur of 5×5, a max jump distance of 20, and a min track length of 8 were used. The measurements were evaluated using the built-in software Nanosight NTA 3.4.

2.5 Imaging

For the scanning electron microscopy (SEM) images, the particles were diluted in MilliQ water to obtain a final concentration of 2×10^8 particles per ml. 10 µl of the diluted sample were transferred to a silicon wafer, allowed to dry, and sputtered with a 3 nm iridium layer. The imaging was performed in a Carl Zeiss 1540 EsB Crossbeam SEM.

2.6 Diffusion measurements

The PFG NMR technique is used to measure diffusion coefficients D of NMR active nuclei. Performing the stimulated echo pulse sequence, magnetic field gradients in the z direction are used to label the nuclear spins of interest by their z position.[58,59] NMR spectra are recorded for different strengths of the magnetic field gradient g and allow the determination of the diffusion

coefficient from the echo attenuation in the integrated intensity I of a resonance peak following[60,61]

$$I(g) = I_0 \cdot \exp(-b(g) \cdot D). \qquad (1)$$

Here, I_0 is the intensity in the absence of a gradient and $b(g)$ is an experimental parameter given by[25,62–64]

$$b(g) = \gamma^2 g^2 \delta_g^2 \left(\Delta - \frac{\pi}{8} \delta_g \right). \qquad (2)$$

It includes the amplitude of the gradient pulse g, the diffusion time Δ, given by the separation of the gradient pulses, and the effective gradient time $\delta_g = 2\delta_s/\pi$, where δ_s describes the duration of the half-sine function gradient pulse. The gyromagnetic ratio γ is dependent on the type of measured nuclei and holds $\gamma_{1H} = 26.75 \times 10^7 \text{ T}^{-1} \text{ s}^{-1}$ and $\gamma_{19F} = 25.18 \times 10^7 \text{ T}^{-1} \text{ s}^{-1}$ for the different nuclei used in the context of this paper.[65] In each PFG NMR experiment, all parameters except g are kept constant, which allows fitting the attenuation of $I(g)$ to obtain the diffusion coefficient.[58,60,61,66,67]

The measurements were performed using a Bruker AVANCE III 400 MHz spectrometer and a Bruker wide-bore magnet. Magnetic field gradients were generated by a DiffBB broadband diffusion probe and a Great60 gradient amplifier from Bruker BioSpin. The instrument allows magnetic field gradient values of up to 17 T m^{-1}. To improve the signal-to-noise ratio, up to 64 signals were added prior to the Fourier transformation. Each experiment was repeated three times. The sample temperature was maintained at 25 °C using a digital PID controller. The temperature was monitored with a thermocouple below the sample, which was calibrated to about ±0.1 K with a high-precision platinum resistor placed in the gas flow at the actual sample position. The maximum temperature drift during measurement was ±0.2 K. The settings used for the measurements mentioned in the context of this manuscript can be found in the SI.

3 Results and discussion

3.1 Diffusion probe fabrication and characterization

We fabricated nanocapsules suitable for diffusion measurements by adapting the internal phase separation method originally developed for production of NMR active PMMA microcapsules.[54–56,68] In what follows, we examined liquid cores of hexadecane with and without fluorinated tracer molecules. In this approach, PMMA, hexadecane, and dichloromethane (DCM) are combined to form a homogeneous hydrophobic phase, which is then dispersed in water to create an oil-in-water emulsion. The obtained micron size droplets are typically stabilized against coalescence using an emulsifier (typically poly(vinyl alcohol) (PVA)). Thus, as the volatile DCM evaporates, PMMA, which is only sparingly soluble in hexadecane, migrates to the interface along with PVA, resulting in stable hexadecane-filled microcapsules.

We hypothesized that to achieve the desired particle diameter of 200 nm it is necessary to reduce the droplet size during emulsification, since the initial droplets serve as templates for
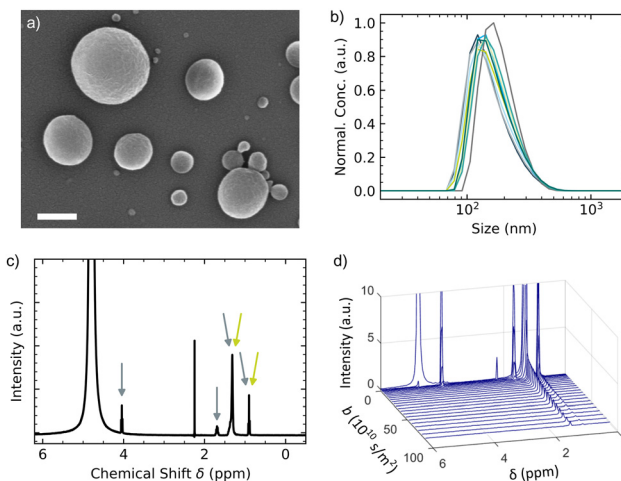

Fig. 2 Characterization of the nanocapsule system. (a) SEM image of the particles. Particles were dried on a silicon wafer and sputtered with a 3 nm iridium layer. The scale bar is 200 nm. (b) Number-weighted particle size distribution of the particles suspended in water, measured by DLS. Each line represents one scan. (c) ^{1}H NMR spectrum of the PMMA-hexadecane particles suspended in an aqueous 0.2% SDS solution at a concentration of 4.1×10^{11} particles per ml. Eight scans were performed. Gray arrows show the peaks that are generated by SDS, green arrows denote the hexadecane signal. (d) Stacked spectra measured by PFG NMR of the sample shown in (c). For the peaks at 1.3 ppm and 0.9 ppm, a fast decay (representing free SDS diffusion) and a slow decay (following the hexadecane diffusion, limited by the diffusion of the particles) is visible, indicating that the encapsulation of hexadecane is successful.

the final particles. Therefore, instead of using the large PVA chains as emulsifiers, we used the smaller sodium dodecyl sulfate (SDS), which offered better control over droplet size at the submicron scale. Additionally, we found that emulsification by ultrasound homogenization combined with the addition of acetone, to reduce foaming, consistently produced stable nanocapsules with the required size distribution. This was confirmed by measuring the size of the obtained particles after evaporation of the DCM. The resulting nanocapsules showed a mean diameter close to the target value of 200 nm, as confirmed by imaging using SEM (Fig. 2a), as well as by DLS as shown in Fig. 2b.

Although reducing the size of PMMA-hexadecane nanocapsules lowers the number of signal-carrying spins, the measurements shown in Fig. 2 confirm that the particles remain detectable by PFG NMR and are suitable for use as diffusion probes. To demonstrate this, we first identified the distinct ^{1}H NMR signals present in the system, and then applied pulsed-field gradients to evaluate which peaks could reliably track nanocapsule motion. Fig. 2c shows the ^{1}H NMR spectrum of the nanocapsules in an aqueous 0.2% SDS solution. In addition to the dominant water peak, which was used to align the spectra by setting it to $\delta = 4.8$ ppm, hexadecane contributes characteristic signals at chemical shifts of $\delta \approx 1.3$ ppm and 0.9 ppm.[69] Further, SDS shows peaks at 4.0 ppm, 1.7 ppm, 1.3 ppm, and 0.9 ppm.[70] Notably, the SDS peaks at 1.3 ppm and 0.9 ppm overlap with signals from hexadecane, the encapsulated oil core of the particles. Peak assignments were made by comparison with reference spectra and established chemical shift values from the literature.[69,70]

After identifying and assigning the different chemical shifts, we performed PFG NMR experiments to evaluate nanocapsule diffusion. As shown in Fig. 2d, signal attenuation with increasing gradient strength reflects molecular mobility: the water peak decays quickly, while signals associated with the particle core persist longer, indicating slower diffusion. This behavior is consistent with the Stokes–Einstein–Sutherland relation, where diffusion scales inversely with particle size. To quantify particle diffusion, we sought to monitor a ^{1}H signal unique to the nanocapsules. However, the proton spectrum shows overlapping signals from both hexadecane and SDS (see Fig. 2c), due to similar methylene ($-CH_2-$) environments, preventing unambiguous assignment of an isolated, particle-specific peak. Nevertheless, by applying a biexponential fit to the signal decay we were able to deconvolve the contributions from the faster-diffusing SDS molecules ($D_1 = (1.51 \pm 0.15) \times 10^{-10}$ m^2 s^{-1}) and the slower nanocapsules ($D_2 = (2.38 \pm 0.04) \times 10^{-12}$ m^2 s^{-1}), yielding a quantitative diffusion coefficient for the particles (see SI for a detailed analysis). In the case of particle suspensions of lower SDS concentration, the SDS contribution can be neglected if the applied gradients have values larger than the threshold where the SDS signal is completely attenuated, which was tested by optical inspection of the echo attenuation plots for the experiments discussed in the following sections.

These results confirm that the nanocapsules are readily detectable and that a characteristic diffusion coefficient can be measured from PFG NMR spectra. We first consider the effect of nanocapsule polydispersity to establish practical measurement limits.

3.2 Limits and resolution of PFG NMR-based nanoparticle tracking

To establish the robustness of using PFG NMR for our nanocapsule diffusion analysis, we examined two factors that can significantly influence its performance: the ability to resolve size distributions in polydisperse samples, and the performance under increasingly viscous conditions. These factors are paramount because they directly test the accuracy of the method against inherent sample heterogeneity and define its practical limits in viscous environments where the diffusion time is a critical constraint.

3.2.1 Obtaining a particle size distribution from PFG NMR measurements. The fabrication of the tracer particles *via* ultrasound homogenization inherently produces a polydisperse population (see Fig. 2), which correlates with a distribution of diffusion coefficients. This effect leads to a curvature of the echo attenuation shown in Fig. 3a, which shows the ^{1}H PFG NMR data for PMMA-hexadecane nanocapsules suspended in water. None of the curves exhibit a single-exponential decay, indicating that the signal arises from particles with varying diffusion behavior. We found this to be consistent for two different proton peaks, both corresponding to hexadecane, after performing three independent measurements. To account for the polydispersity, we followed Röding *et al.*[71] and assumed a gamma distribution of diffusion coefficients $P(D;\kappa,\theta)$. The gamma distribution gives comparable results to the log-normal
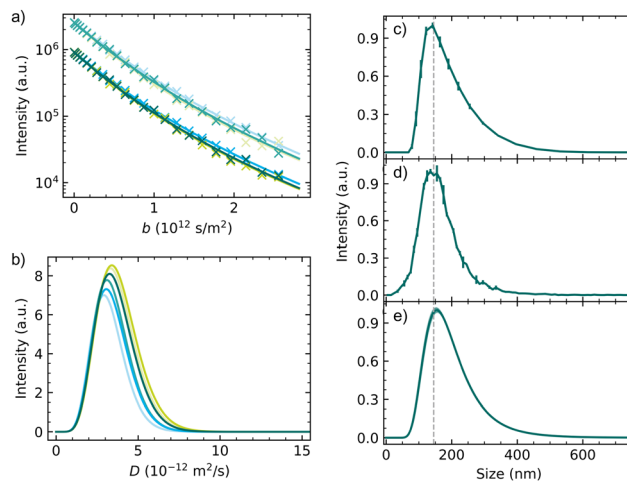

Fig. 3 Results of PFG NMR measurements using the number-weighted gamma distribution and comparison to other methods. (a) Echo attenuation measured by ^{1}H PFG NMR of the PMMA-hexadecane particles suspended in water, evaluated using the number-weighted gamma distribution model. Each data set of the two hexadecane peaks for the three measurements is evaluated individually. Parameters for PFG NMR are Δ = 50 ms, δ_g = 2.5 ms, 32 scans per gradient strength, and a particle concentration of 5×10^{11} particles per ml. (b) From the fitting parameters, the number-weighted gamma distribution of diffusion coefficients is obtained, yielding a mean diffusion coefficient of $\langle D \rangle = 3.55 \times 10^{-12}$ m^2 s^{-1} and a standard deviation of $\sigma_D = 1.15 \times 10^{-12}$ m^2 s^{-1}. (c) PSD of the particles measured by DLS, the curve shows the averaged result of the ten measurements presented in Fig. 2b. (d) PSD measured by NTA, averaged over two measurements. (e) PSD measured by PFG NMR as obtained from change of variables of the curves shown in subfigure (b). The average of the six curves is shown here. The error bars in (c) and (d) and the shaded area in (e) represent the standard errors of the mean.

distribution and is hence assumed to be a reasonable model for the distribution of diffusion coefficients in case of polydispersity. Moreover, it is analytically solvable for a PFG NMR intensity attenuation.[71,72] However, this approach yields a volume weighted distribution of diffusion coefficients, since the signal intensity of each particle is dependent on the number of spins inside it and hence on its inner volume. This leads to an over-representation of larger particles in the measured signal. We therefore introduce here a modified gamma distribution that compensates this volume effect by applying a normalization approach:

$$\tilde{P}(D;\kappa,\theta) = P(D;\kappa,\theta) \cdot \frac{D^3}{D_0^{\,3}} = \frac{D^{\kappa+2}}{D_0^{\,3}} \frac{\exp(-D/\theta)}{\Gamma(\kappa)\theta^\kappa}, \qquad (3)$$

where $\Gamma(x)$ is the gamma function, and κ and θ are shape and scale parameters, respectively. D_0 is chosen to normalize the distribution. The PFG NMR signal attenuation weighted by this distribution of diffusion coefficients then becomes

$$I(b) = I_0 \cdot \int_0^\infty P(D) \exp(-bD)\mathrm{d}D = I_0(1 + b\theta)^{-\kappa} \qquad (4)$$

as shown in the SI.

By obtaining the parameters κ and θ from the fit, it is possible to calculate the mean diffusion coefficient $\langle D \rangle$ and its standard deviation σ_D of the distribution $\tilde{P}(D;\kappa,\theta)$. Fig. 3b

shows the distributions of diffusion coefficients calculated from the fits to the echo attenuation of the particles in water shown in Fig. 3a. Each curve corresponds to the evaluation of the same color in subfigure (a). The curves shown here are not normalized, but in the following their mean is used.

In order to asses the validity of this approach, we convert the output of the analysis to a particle size distribution (PSD) using the Stokes–Einstein–Sutherland equation $D = k_B T/6\pi\eta R$. As shown in the SI, from the distribution of diffusion coefficients one can calculate the distribution of radii $\tilde{P}(R;\kappa,\theta)$ with characteristic mean particle radius $\langle R \rangle$ and standard deviation σ_R. The averaged distribution of particle sizes in water as calculated from the distribution of diffusion coefficients in Fig. 3b is shown in Fig. 3e, where the shaded area represents the standard error of the mean of the six evaluations.

The PSD curves obtained by complementary methods are shown in Fig. 3c (DLS) and Fig. 3d (NTA), where the error bars represent the standard error of the mean. All three PSD plots show a single maximum, which represents a population of one size. The positions of the maxima are well aligned, despite slight differences in the shape of the curves. This shows that the PFG NMR diffusion measurements closely match conventional light-based methods, when a distribution of diffusion coefficients is used for size distribution measurements.

3.2.2 Particle diffusion in viscous systems. In samples of higher viscosity, longer diffusion times are required to observe meaningful displacements of the diffusing particles. However, the range of operation is limited by relaxation processes. We prepared a series of aqueous glycerol solutions (0–80% v/v) to systematically increase the sample viscosity over two orders of magnitude.[73] The distinct ^{1}H NMR signals of the hexadecane core in this environment allowed for a clear, interference-free measurement of particle diffusion, as the glycerol signals in the ^{1}H NMR spectrum do not overlap with the hexadecane peaks.[74] The hexadecane signal was evaluated to obtain the particle diffusion as described above.

The glycerol solutions are, as expected, homogeneous and isotropic, as the diffusion coefficient is independent of the diffusion time (see SI). The diffusion time was adjusted for the different samples to compensate for slower diffusion in media of higher viscosity and be able to compare the diffusion coefficient in the glycerol solutions. The diffusion time was set to Δ = 100 ms and increased to 150 ms and 500 ms for the solutions of 60% and 80% glycerol, respectively.

As expected, with increasing viscosity there is a systematic decrease in nanocapsule mobility. This trend is directly visible in the raw NMR echo attenuation data in Fig. 4a, which presents exemplary plots of the NMR echo attenuation for the hexadecane peak at $\delta \approx 1.3$ ppm. By fitting these curves with a number-weighted gamma distribution, we extracted the mean diffusion coefficient for each sample, which shows a smooth, monotonic decrease with increasing glycerol content (Fig. 4b). It has to be noted that the fit model of the number-weighted gamma distribution is sensitive to small deviations in the measured data points, and hence does not converge in all instances (data not shown).
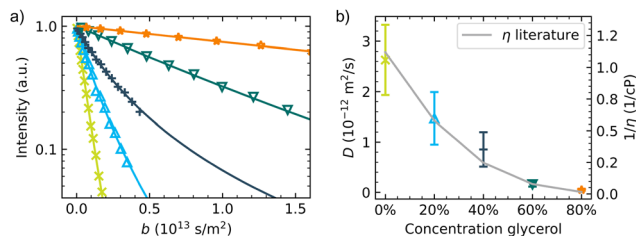

Fig. 4 Results of the ^{1}H PFG NMR measurements of the PMMA-hexadecane particles in aqueous glycerol solutions of different concentrations. Each sample was measured three times and evaluated using the number-weighted gamma distribution model for each individual measurement. (a) Exemplary echo attenuation plots of the measurements using Δ = 100 ms and δ_g = 5 ms. A particle concentration of 5×10^{11} particles per ml was used and 32 scans were performed. To compensate for the higher viscosity in the samples of 60% and 80% glycerol, the diffusion times were increased to 150 ms and 500 ms, respectively. (b) Averaged mean diffusion coefficients and their standard deviation (shown as error bars) as obtained from the number-weighted gamma distribution fit on the measurements in glycerol solutions. The concentration given on the x axis refers to a volume concentration of glycerol. The inverse of the viscosity for aqueous glycerol solutions as given in the literature[73] is shown in gray as a guide to the eye. The two y axes are not correlated.

The NMR-derived viscosities obtained from fits of the Stokes–Einstein–Sutherland relation to the data show excellent agreement with established literature values for glycerol–water mixtures[73] that are indicated on the right hand axis in Fig. 4b. The derived viscosity values are shown and compared to the literature data in SI Table S2. This strong correlation confirms that our approach accurately captures diffusion physics even as the viscosity increases nearly 100-fold compared to water. The longitudinal relaxation time of the hexadecane is in the range of $T_1 \approx 700$–800 ms (see SI), hence the upper limit of the diffusion time is $\Delta < 800$ ms to prevent increased signal loss. This puts a limit to the range of viscosities that can be investigated. This validation establishes the suitability of the technique for probing structurally complex systems, such as the hydrogels, which we investigate next.

3.3 Measuring hydrogel mesh size by PFG NMR

To probe the microstructure of hydrogels, we focused on agarose and methacrylated hyaluronic acid (HAMA) hydrogels. HAMA particularly shows excellent biocompatibility and is widely used in biomedical applications like tissue engineering[75–81] and drug delivery.[76,82] For these applications, the microstructure of the polymer network is of critical interest. This structure is typically characterized by two parameters, pore size and mesh size. Mesh size represents the characteristic, nanometer-scale distance between polymer cross-links, while pore size refers to the micro- to macroscale voids in a gel, which can be introduced during suitable gel fabrication.[49,50,83] Experimentally determining the mesh size is challenging, and reported mesh sizes yield highly variable results depending on the method. For example, scanning electron microscopy (SEM) images reported pore sizes in the micron to millimeter range, but this technique requires sample dehydration, which is expected to alter the native structure.[84–88] Conversely, indirect methods relying on swelling measurements

estimated the mesh size to be in range between tens and hundreds of nanometers up to microns, but these are based on models with simplifying assumptions.[52,53,89]

The diffusion of nanoscale probes instead provides a potential direct and robust means to assess the mesh size.[6,8,50,90] By tracking particle displacements over short length scales, PFG NMR is inherently sensitive to the nanometer-scale constraints of the polymer mesh, thereby providing a direct measure of mesh size. In complex environments like hydrogels, obstacles like a polymer network slow down particle movement, and the mean squared displacement (MSD) of the particle reaches a maximum value determined by the dimensions of the confining geometry,[25,60,91] giving rise to an apparent diffusion coefficient D_{app}. As depicted in Fig. 5a, on a short timescale (small Δ), diffusing particles move nearly unhindered ($D_{app} \approx D_0$). For increasing diffusion time (intermediate Δ), however, the effect of the restricting geometry leads to an apparently lower diffusion coefficient. In the long-term limit (long Δ), the diffusion coefficient can reach a constant value or, if the species is enclosed in a cavity, approach zero ($D_{app} \to 0$). The time-dependence of the apparent diffusion coefficient therefore gives information about the behavior of the particle under confinement.

The fundamental principle of this technique is thus to probe the mesh size of the hydrogel by observing how the apparent diffusion coefficient D_{app} of a nanocapsule changes with the measurement time Δ. However, to successfully apply this principle in a hydrogel requires overcoming two experimental challenges. First, a significant hurdle arises because the standard PFG NMR approach using protons (^{1}H) is complicated in the hydrogel matrix as shown in the spectrum of particles in a HAMA gel in Fig. S5, requiring a background-free detection method to permit observation of the nanocapsules' diffusion. Second, interpretation of the data depends on the degree of confinement: for weakly confined particles, the measured signal reflects the movement of the particle through the mesh, while for strongly confined or trapped particles, the translational motion becomes minimal, and the signal can be dominated by the internal diffusion of liquid within the nanocapsule itself. Differentiating these effects is critical for an accurate determination of the mesh size.

To address the first challenge of overlapping signals, we developed an alternative approach using ^{19}F NMR. We introduced a fluorinated reporter molecule (a fluorinated silane 1H,1H,2H,2H-perfluorooctyltriethoxysilane, POTS; molecular structure is shown in the SI) into the nanocapsule core. This strategy offers key advantages: [19]F is virtually absent in biological matrices and the chosen molecule provides a strong NMR signal which increases the detection sensitivity. The resulting ^{19}F NMR spectrum is shown in Fig. 5b, where both peaks correspond exclusively to the POTS reporter molecule within the nanocapsule.

Before applying the nanocapsules to the hydrogels, we first validate the use of the fluorinated tracer, measured by ^{19}F PFG NMR, against ^{1}H signals. As shown in the SI, ^{19}F PFG NMR measurements of the PMMA-hexadecane particles including POTS yield diffusion coefficients consistent with those obtained using ^{1}H NMR. Crucially, the ^{19}F approach simplifies the analysis by eliminating any signal overlap.

Having established a reliable, background-free method to track our nanocapsules, we now address the second challenge: deconvoluting the true diffusion of the particle in highly confined environments. For that, we investigated the diffusion of the nanocapsules in a well-defined control system where the mesh size can be assumed to be small enough to completely immobilize the particles. All measurements in the hydrogel samples were analyzed using an exponential decay fit to the echo attenuation instead of the number-weighted gamma distribution model due to the low signal to noise ratio of the collected data. Hence, the error bars discussed in the following do not represent a standard deviation of the distribution of diffusion coefficients, but the fitting error of the diffusion coefficient.

We first measured the PFG NMR signal from nanocapsules in a high-concentration (3%) agarose gel, a system designed to completely immobilize the particles. The measured displacement
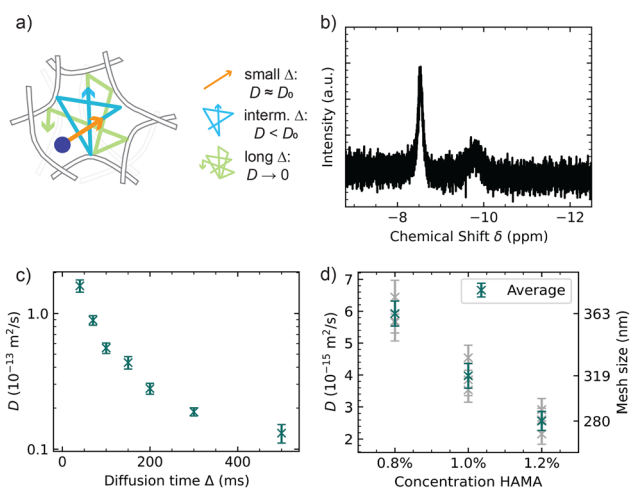

Fig. 5 Evaluation of the diffusion of PMMA-hexadecane particles filled with POTS in hydrogels to investigate their microstructure. (a) Expected time-dependent diffusion coefficient for particles trapped in a cavity. Dark green lines represent the gel fibres, curvy lines show the random walk of a particle for short diffusion times Δ (orange), intermediate Δ (light blue), and long Δ (light green). (b) ^{19}F NMR spectrum of the particles in water at a concentration of 5×10^{11} particles per ml. 64 scans were recorded. (c) Apparent diffusion coefficients of PMMA-hexadecane particles filled with POTS measured using ^{19}F PFG NMR in a 0.75% agarose gel. The values of D are determined using an exponential fit on the echo attenuation. The mean value is obtained from two measurements, and its uncertainty is shown as error bars. The radius of the particles was determined beforehand to be 177 nm using a gamma distribution fit on ^{1}H PFG NMR data of the particles in water. The measurements were performed at $\Delta = 500$ ms and $\delta_g = 2.5$ ms. 64 scans were performed. (d) Diffusion coefficients measured by ^{19}F PFG NMR using the POTS signal in HAMA gels of different concentration of the HAMA polymer. The particle radius is 120 nm as measured by ^{1}H PFG NMR. The measurements were performed at $\Delta = 500$ ms, $\delta_g = 5$ ms, and 64 scans. Three measurements were performed and averaged. The error bars denote the uncertainty of the mean diffusion coefficient. The gray data points show the individual measurements. The mesh size indicated on the right hand axis is estimated using eqn (6).

should then be independent of the diffusion time Δ for the time scales probed by PFG NMR and correspond solely to the reporter molecule motion within the core of the nanocapsule. A precise prediction requires knowledge of the inner core diameter. Based on our analysis (see SI), the shell thickness is estimated to be approximately half the outer radius of the particle. For the particles under study, which have a total diameter of 354 nm (radius of 177 nm), this results in a shell thickness of $\sim$88 nm and an inner core diameter of $\sim$177 nm. According to theory,[25,91] the expected internal displacement is approximately 0.6 times this inner core diameter, *i.e.* $\sim$106 nm.

Diffusion measurements at 500 ms and 100 ms and different measurement parameters revealed mean covered distances of $\sqrt{\langle r^2 \rangle} = 81$ nm and 122 nm, respectively (details are given in the SI). This excellent agreement between the experimental measurement and the theoretical prediction provides direct proof that the particles are indeed immobilized by the dense gel and that the resulting signal is a reliable measure of internal diffusion.

Having quantified the internal diffusion, we investigated a system with larger pores: a 0.75% agarose gel. In this environment, the nanocapsules are expected to be confined within a cavity in the gel mesh that is larger than their own diameter. Consequently, the measured MSD should now be a combination of two distinct motions: the translational diffusion of the particle within its confining pore and the previously characterized internal diffusion of the core liquid.

PFG NMR measurements of the particles in the 0.75% agarose gel yield a mean covered distance in the range of 183 nm to 198 nm for diffusion times between 40 ms and 500 ms. The corresponding apparent diffusion coefficients are shown in Fig. 5c. Crucially, this displacement value does not increase with longer diffusion times, confirming that the particles are effectively trapped within individual pores. This measured displacement is significantly larger than the $\sim$106 nm attributed to internal diffusion alone, indicating that the particle itself is undergoing translational motion within a pore larger than its own diameter. To estimate the mesh size, the confining voids are modeled as spherical boundaries in analogy to existing literature models.[68,91–93] For small values of the gradient strength and duration (denoted as the combined value $q = \gamma \delta_g g$) and for long-term diffusion, the model assumes that the position of the particles is independent of the starting position, and the probability of finding the particle at a certain position is only dependent on the density distribution inside the cavity. The diffusion coefficient is then only dependent on the radius a of the spherical pore as given in ref. 68 and 91–93. In this model, the radius a of the space explored by the liquid core is calculated from the measured apparent diffusion coefficient D and the diffusion time Δ:

$$a = \sqrt{5\Delta D} \qquad (5)$$

The total mesh size ξ must also include the shell thickness of the particle R_{shell}, which acts as a physical spacer between the liquid core and the hydrogel network. The mesh size is therefore the diameter of the explored space plus the shell thickness on both sides:

$$\xi = 2a + 2R_{shell} \qquad (6)$$

This analysis yields a mesh size for the 0.75% agarose gel of approximately (525 ± 165) nm. The uncertainty of the mesh size was estimated using error propagation including the standard deviation of the diffusion coefficient and the particle radius, as well as the uncertainty of the core radius. Here, the standard deviation of the particle size provides the biggest contribution. Despite the large uncertainty, the estimated mesh size is in agreement with geometric considerations, as a freely diffusing particle would cover $\sim$700 nm in the time frame of the smallest measured diffusion time of 40 ms. Since at this diffusion time the diffusion is clearly slowed down, this confirms that the mesh size is well below this value. Nevertheless, it has to be mentioned that this model does not account for a distribution of mesh sizes in the hydrogel.

Building on the insights from the model agarose systems, we applied our fully validated method to HAMA gels. We investigated the apparent diffusion of PMMA-hexadecane particles by ^{19}F PFG NMR in HAMA gels of different concentrations. The particles used here were analyzed using the number-weighted gamma distribution model fit on the ^{1}H PFG NMR measurement of the particles suspended in water and found to have a size around 240 nm. The resulting diffusion coefficients of the particles in HAMA gels, measured by ^{19}F PFG NMR for a diffusion time of 500 ms, are shown in Fig. 5d. A clear trend was observed: the apparent diffusion coefficient as evaluated from an exponential fit to the echo attenuation decreased as the polymer concentration increased, which is consistent with the expected reduction in gel mesh size and particle mobility. A closer evaluation confirms that, similar to the agarose system, the particles are trapped within individual pores. The mesh sizes for the different HAMA concentrations were estimated using the same analysis, with the results indicated on the right-hand axis in Fig. 5d and a measurement uncertainty of approximately 50 nm. It is important to note that these HAMA gel samples are at the lower limit of the diffusion coefficient that our method can detect under the present experimental conditions due to the need of high gradient intensity to resolve small displacements. A discussion of possible artifacts for other measurement conditions is presented in the SI. Consequently, the evaluated mesh size of the HAMA gel should be interpreted as a reliable maximum value of the true mesh size in the hydrated state. The main finding is that the particles are trapped inside the HAMA gels, with an effective mesh size on the order of the particle diameter that systematically decreases as the gel concentration increases. The reported mesh sizes of around 200 nm represent the lower limit of the given measurement system using the 200 nm sized particles. On the other hand, we estimate the upper limit of mesh sizes that can be reliably measured using this system to be in the range of six times the particle size (*e.g.* 1200 nm, see SI).

Conclusions

In this work, we demonstrated a robust PFG NMR-based approach for quantifying the microstructure of hydrogels in their native, hydrated state. Using custom-designed, liquid-filled nano-capsules, we directly measured the effective mesh size of complex polymer networks such as HAMA gels, providing quantitative insight how the microstructure relates to composition.

Two key analytical challenges were addressed. First, we resolved the issue of signal interference in proton-rich matrices by introducing fluorine-19 (^{19}F) reporters to the liquid core of our nanocapsules, enabling background-free detection. Second, we developed a rigorous correction for the internal liquid diffusion within the nanocapsules, which is important when particle mobility is restricted. By quantifying and sub-tracting this contribution, we isolated the translational motion of the particles within the hydrogel mesh.

In addition, we introduced a mathematical framework for extracting a distribution of diffusion coefficients from PFG NMR measurements, accounting for the inherent polydispersity of the tracer particles. By fitting a volume-corrected gamma distribution model to the echo attenuation data, we obtained accurate diffusion coefficient distributions, which were further converted into particle size distributions using the Stokes–Einstein–Sutherland equation. The resulting distributions aligned well with independent measurements from DLS and NTA, demonstrating the reliability and quantitative power of the approach.

The presented method offers a practical, non-invasive framework for probing the nanoscale architecture of soft biomaterials. It opens new avenues not only for hydrogel mesh characterization, but also for studying colloidal transport in crowded environments.

The particles hold significant potential for broader applications. The ability to functionalize the surface of the nanocapsules enables studies of how specific particle–matrix interactions – such as electrostatic or hydrophobic effects – influence diffusion. This makes the system highly relevant for mimicking biologically active carriers, exploring drug delivery mechanisms, or tracking active particles in tissue-like environments. Reducing the size of the particles could further extend the method to hydrogels with finer microstructures. Indeed, using liquid filled nanocapsules of 200 nm address an experimental gap, complementing studies that use either diffusing molecules[16,21] or larger, micron size capsules.[35–41] This regime is ideal for characterizing the lattices of many hydrogels.

The particles could be adapted to probe a different size regime. By fabricating nanoprobes that are significantly smaller than the hydrogel mesh, one could study hindered diffusion rather than confinement. In such a scenario, the diffusion analysis could provide access to complementary structural parameters, such as network tortuosity and surface-to-volume ratio, as described in literature.[94,95] However, such an analysis requires that one can rigorously account for the effects of particle polydispersity and shell thickness.

Importantly, this technique also provides access to media that are inaccessible to optical methods. Its insensitivity to optical clarity and labeling requirements makes PFG NMR a uniquely powerful approach for probing transport phenomena in turbid, opaque, or light-sensitive biological samples.

For reliable application, a careful selection of the NMR parameters is crucial. The diffusion time Δ must be sufficiently long to probe environmental structure, but shorter than the longitudinal relaxation time that was measured to be in a range of $T_1 \approx 700$–800 ms. Likewise, the gradient duration δ_g should remain below ~ 10 ms to avoid signal loss due to transverse relaxation (T_2) and artifacts arising from strong gradient intensities.

Overall, this work establishes a powerful method for investigating the microstructure of soft materials, with particular promise for complex, opaque, or biologically relevant environments.

Author contributions

Conflicts of interest

There are no conflicts to declare.

Data availability

The data supporting this article have been included as part of the supplementary information (SI). Supplementary information is available. See DOI: **https://doi.org/10.1039/d5sm00756a**.

Acknowledgements

Notes and references

1 M. D'Anca, C. Fenoglio, M. Serpente, B. Arosio, M. Cesari, E. A. Scarpini and D. Galimberti, *Front. Aging Neurosci.*, 2019, **11**, 232.

2 N. Kastelowitz and H. Yin, *ChemBioChem*, 2014, **15**, 923–928.

3 F. Etoc, E. Balloul, C. Vicario, D. Normanno, D. Liße, A. Sittner, J. Piehler, M. Dahan and M. Coppey, *Nat. Mater.*, 2018, **17**, 740–746.

4 O. Lieleg and K. Ribbeck, *Trends Cell Biol.*, 2011, **21**, 543–551.

5 F. V. Lavrentev, V. V. Shilovskikh, V. S. Alabusheva, V. Y. Yurova, A. A. Nikitina, S. A. Ulasevich and E. V. Skorb, *Molecules*, 2023, **28**, 5931.

6 B. Amsden, *Macromolecules*, 1998, **31**, 8382–8395.

7 B. Amsden, *Macromolecules*, 1999, **32**, 874–879.

8 B. G. Amsden, *Macromolecules*, 2022, **55**, 8399–8408.

9 N. R. Richbourg and N. A. Peppas, *Prog. Polym. Sci.*, 2020, **105**, 101243.

10 G. Majer and A. Southan, *J. Chem. Phys.*, 2017, **146**, 225101.

11 G. Majer and A. Southan, *PFG-NMR studies of ATP diffusion in PEG-DA hydrogels and aqueous solutions of PEG-DA polymers*.

12 G. Palazzo and L. Paduano, *Colloidal Foundations of Nanoscience*, Elsevier, 2022, pp. 257–287.

13 Y. J. Yu, Y. H. Kim, K. Na, S. Y. Min, O. K. Hwang, K. Da Park, D. Y. Kim, S. H. Choi, R. D. Kamm, S. Chung and J. A. Kim, *Lab Chip*, 2018, **18**, 2604–2613.

14 L. P.-H. Li, A.-W. Li, W.-Y. Chen, C.-H. Cheng, Y.-B. Chen and C.-Y. Liu, *Adv. Photonics Res.*, 2024, **5**, 2400031.

15 D. W. de Kort, J. P. M. van Duynhoven, F. J. M. Hoeben, H. M. Janssen and H. van As, *Anal. Chem.*, 2014, **86**, 9229–9235.

16 D. W. de Kort, J. P. van Duynhoven, H. van As and F. Mariette, *Trends Food Sci. Technol.*, 2015, **42**, 13–26.

17 D. W. de Kort, E. Schuster, F. J. M. Hoeben, R. Barnes, M. Emondts, H. M. Janssen, N. Lorén, S. Han, H. van As and J. P. M. van Duynhoven, *Langmuir*, 2018, **34**, 11110–11120.

18 N. Lorén, L. Shtykova, S. Kidman, P. Jarvoll, M. Nydén and A.-M. Hermansson, *Biomacromolecules*, 2009, **10**, 275–284.

19 R. Mashiach, L. Avram and A. Bar-Shir, *Nano Lett.*, 2022, **22**, 8519–8525.

20 G. Lafitte, K. Thuresson, P. Jarwoll and M. Nydén, *Langmuir*, 2007, **23**, 10933–10939.

21 G. Lafitte, O. Söderman, K. Thuresson and J. Davies, *Biopolymers*, 2007, **86**, 165–175.

22 T. Brenner and S. Matsukawa, *Int. J. Biol. Macromol.*, 2016, **92**, 1151–1154.

23 F. Franconi, L. Lemaire, J.-C. Gimel, S. Bonnet and P. Saulnier, *J. Controlled Release*, 2021, **337**, 155–167.

24 L. Jowkarderis and T. G. M. van de Ven, *Soft Matter*, 2015, **11**, 9201–9210.

25 W. S. Price, *NMR Studies of Translational Motion*, Cambridge University Press, 2009.

26 L. Liang, Y. Ji, K. Chen, P. Gao, Z. Zhao and G. Hou, *Chem. Rev.*, 2022, **122**, 9880–9942.

27 M. H. Blees, J. M. Geurts and J. C. Leyte, *Langmuir*, 1996, **12**, 1947–1957.

28 C. Leal, S. Rögnvaldsson, S. Fossheim, E. A. Nilssen and D. Topgaard, *J. Colloid Interface Sci.*, 2008, **325**, 485–493.

29 F. Odeh, N. Heldt, M. Gauger, G. Slack and Y. Li, *J. Dispersion Sci. Technol.*, 2006, **27**, 665–669.

30 M. Valentini, A. Vaccaro, A. Rehor, A. Napoli, J. A. Hubbell and N. Tirelli, *J. Am. Chem. Soc.*, 2004, **126**, 2142–2147.

31 W. Zhang, K. J. Haman, J. M. Metzger, B. J. Hackel, F. S. Bates and T. P. Lodge, *Langmuir*, 2017, **33**, 12624–12634.

32 U. Olsson, K. Nakamura, H. Kunieda and R. Strey, *Langmuir*, 1996, **12**, 3045–3054.

33 A. Caria, O. Regev and A. Khan, *J. Colloid Interface Sci.*, 1998, **200**, 19–30.

34 T. Kawaguchi, R. Kita, N. Shinyashiki, S. Yagihara and M. Fukuzaki, *Trans. Mater. Res. Soc. Jpn.*, 2016, **41**, 359–362.

35 H. Wassenius and P. T. Callaghan, *J. Magn. Reson.*, 2004, **169**, 250–256.

36 H. Wassenius and P. T. Callaghan, *Eur. Phys. J. E:Soft Matter Biol. Phys.*, 2005, **18**, 69–84.

37 E. O. Fridjonsson, J. D. Seymour and S. L. Codd, *Phys. Rev. E: Stat., Nonlinear, Soft Matter Phys.*, 2014, **90**, 010301.

38 E. O. Fridjonsson and J. D. Seymour, *Chem. Eng. Sci.*, 2016, **153**, 165–173.

39 T. R. Brosten, E. O. Fridjonsson, S. L. Codd and J. D. Seymour, *J. Colloid Interface Sci.*, 2010, **349**, 384–391.

40 J. R. Brown, J. D. Seymour, S. L. Codd, E. O. Fridjonsson, G. R. Cokelet and M. Nydén, *Phys. Rev. Lett.*, 2007, **99**, 240602.

41 J. R. Brown, E. O. Fridjonsson, J. D. Seymour and S. L. Codd, *Phys. Fluids*, 2009, **21**, 093301.

42 G. A. Ferreira, W. Loh, D. Topgaard, O. Söderman and L. Piculell, *Polymers*, 2021, **13**, 3265.

43 S. Fu, Y. Wang, X. Xia and J. C. Zheng, *NanoImpact*, 2020, **20**, 100261.

44 A. George, P. A. Shah and P. S. Shrivastav, *Int. J. Pharm.*, 2019, **561**, 244–264.

45 A. Gordillo-Galeano and C. E. Mora-Huertas, *Eur. J. Pharm. Biopharm.*, 2018, **133**, 285–308.

46 Y. Liu, Y. Liang, J. Yuhong, P. Xin, J. L. Han, Y. Du, X. Yu, R. Zhu, M. Zhang, W. Chen and Y. Ma, *Drug Des., Dev. Ther.*, 2024, **18**, 1469–1495.

47 F. D. Martinez-Garcia, T. Fischer, A. Hayn, C. T. Mierke, J. K. Burgess and M. C. Harmsen, *Gels*, 2022, **8**, 535.

48 P. Patel and P. Thareja, *Eur. Polym. J.*, 2022, **163**, 110935.

49 J. Karvinen, T. O. Ihalainen, M. T. Calejo, I. Jönkkäri and M. Kellomäki, *Mater. Sci. Eng., C*, 2019, **94**, 1056–1066.

50 N. A. Peppas, Y. Huang, M. Torres-Lugo, J. H. Ward and J. Zhang, *Annu. Rev. Biomed. Eng.*, 2000, **2**, 9–29.

51 U. S. K. Madduma-Bandarage and S. V. Madihally, *J. Appl. Polym. Sci.*, 2021, **138**, 50376.

52 J. Baier Leach, K. A. Bivens, C. W. Patrick and C. E. Schmidt, *Biotechnol. Bioeng.*, 2003, **82**, 578–589.

53 B. S. Spearman, N. K. Agrawal, A. Rubiano, C. S. Simmons, S. Mobini and C. E. Schmidt, *J. Biomed. Mater. Res., Part A*, 2020, **108**, 279–291.

54 A. Loxley and B. Vincent, *J. Colloid Interface Sci.*, 1998, **208**, 49–62.

55 V. Eriksson, L. Beckerman, E. Aerts, M. Andersson Trojer and L. Evenäs, *Langmuir*, 2023, **39**, 18003–18010.

56 V. Eriksson, S. Edegran, M. Croy, L. Evenäs and M. Andersson Trojer, *J. Colloid Interface Sci.*, 2024, **662**, 572–582.

57 B. Ananthanarayanan, Y. Kim and S. Kumar, *Biomaterials*, 2011, **32**, 7913–7923.

58 E. O. Stejskal and J. E. Tanner, *J. Chem. Phys.*, 1965, **42**, 288–292.

59 J. E. Tanner, *J. Chem. Phys.*, 1970, **52**, 2523–2526.

60 W. S. Price, *Concepts Magn. Reson.*, 1997, **9**, 299–336.

61 W. S. Price, *Concepts Magn. Reson.*, 1998, **10**, 197–237.

62 W. S. Price and P. W. Kuchel, *J. Magn. Reson.*, 1991, **94**, 133–139.

63 G. Majer and K. Zick, *J. Chem. Phys.*, 2015, **142**, 164202.

64 J.-P. Günther, G. Majer and P. Fischer, *J. Chem. Phys.*, 2019, **150**, 124201.

65 W. Schlegel, C. P. Karger and O. Jäkel, *Medizinische Physik*, Springer Berlin Heidelberg, Berlin, Heidelberg, 2018.

66 G. H. Sørland, *Dynamic Pulsed-Field-Gradient NMR*, Springer Berlin Heidelberg, Berlin, Heidelberg, 2014, vol. 110.

67 H. C. Torrey, *Phys. Rev.*, 1956, **104**, 563–565.

68 H. Wassenius, M. Nydén and B. Vincent, *J. Colloid Interface Sci.*, 2003, **264**, 538–547.

69 X.-Y. Li, R. Shang, M.-C. Fu and Y. Fu, *Green Chem.*, 2015, **17**, 2790–2793.

70 Z. Yang, J. Cui and B. Yin, *Water, Air, Soil Pollut.*, 2018, **229**, 304.

71 M. Röding, D. Bernin, J. Jonasson, A. Särkkä, D. Topgaard, M. Rudemo and M. Nydén, *J. Magn. Reson.*, 2012, **222**, 105–111.

72 B. Håkansson, M. Nydén and O. Söderman, *Colloid Polym. Sci.*, 2000, **278**, 399–405.

73 N.-S. Cheng, *Ind. Eng. Chem. Res.*, 2008, **47**, 3285–3288.

74 A. D. Wexler, J. Woisetschläger, U. Reiter, G. Reiter, M. Fuchsjäger, E. C. Fuchs and L. Brecker, *ACS Omega*, 2020, **5**, 22057–22070.

75 X. Jia, J. A. Burdick, J. Kobler, R. J. Clifton, J. J. Rosowski, S. M. Zeitels and R. Langer, *Macromolecules*, 2004, **37**, 3239–3248.

76 V. G. Muir and J. A. Burdick, *Chem. Rev.*, 2021, **121**, 10908–10949.

77 J. Lu, Z. Gao, W. He and Y. Lu, *J. Orthop. Transl.*, 2025, **50**, 111–128.

78 C. C. L. Schuurmans, M. Mihajlovic, C. Hiemstra, K. Ito, W. E. Hennink and T. Vermonden, *Biomaterials*, 2021, **268**, 120602.

79 L. Ouyang, C. B. Highley, C. B. Rodell, W. Sun and J. A. Burdick, *ACS Biomater. Sci. Eng.*, 2016, **2**, 1743–1751.

80 G.-W. Hong, J. Wan, Y. Park, J. Yoo, H. Cartier, S. Garson, D. Haykal and K.-H. Yi, *Polymers*, 2024, **16**, 2739.

81 A. A. Sanchez, F. C. Teixeira, P. Casademunt, I. Beeren, L. Moroni and C. Mota, *Biofabrication*, 2025, **17**, 025013.

82 G. D'Arrigo, C. Di Meo, E. Geissler, T. Coviello, F. Alhaique and P. Matricardi, *Colloid Polym. Sci.*, 2012, **290**, 1575–1582.

83 N. Annabi, J. W. Nichol, X. Zhong, C. Ji, S. Koshy, A. Khademhosseini and F. Dehghani, *Tissue Eng., Part B*, 2010, **16**, 371–383.

84 J. Hu, C. Li, S. Jin, Y. Ye, Y. Fang, P. Xu and C. Zhang, *Front. Bioeng. Biotechnol.*, 2022, **10**, 950625.

85 Y. Zhou, Z. Gu, J. Liu, K. Huang, G. Liu and J. Wu, *Carbohydr. Polym.*, 2020, **230**, 115640.

86 B. Teong, S.-C. Wu, C.-M. Chang, J.-W. Chen, H.-T. Chen, C.-H. Chen, J.-K. Chang and M.-L. Ho, *J. Biomed. Mater. Res., Part B*, 2018, **106**, 808–816.

87 B. Velasco-Rodriguez, T. Diaz-Vidal, L. C. Rosales-Rivera, C. A. García-González, C. Alvarez-Lorenzo, A. Al-Modlej, V. Domínguez-Arca, G. Prieto, S. Barbosa, J. F. A. Soltero Martínez and P. Taboada, *Int. J. Mol. Sci.*, 2021, **22**, 6758.

88 Y. Gao, W. Dai, S. Li, X. Zhao, J. Wang, W. Fu, L. Guo, Y. Fan and X. Zhang, *J. Mater. Chem. B*, 2023, **11**, 10029–10042.

89 S. Yu, Z. Zeng, C. Guo, J. Jiang, D. Pei, D. Lu and Z. Geng, *Chem. Pap.*, 2021, **75**, 4093–4098.

90 M. Vigata, C. Meinert, D. W. Hutmacher and N. Bock, *Pharmaceutics*, 2020, **12**, 1188.

91 P. T. Callaghan, *Translational Dynamics and Magnetic Resonance*, Oxford University Press, 2011.

92 A. Pochert, D. Schneider, J. Haase, M. Linden and R. Valiullin, *Langmuir*, 2015, **31**, 10285–10295.

93 J. Kärger, M. Avramovska, D. Freude, J. Haase, S. Hwang and R. Valiullin, *Adsorption*, 2021, **27**, 453–484.

94 L. L. Latour, P. P. Mitra, R. L. Kleinberg and C. H. Sotak, *J. Magn. Reson., Ser. A*, 1993, **101**, 342–346.

95 M. Urbańczyk, Y. Kharbanda, O. Mankinen and V.-V. Telkki, *Anal. Chem.*, 2020, **92**, 9948–9955.